Purdue University
Purdue e-Pubs

International Compressor Engineering Conference

School of Mechanical Engineering

2014

Development and Testing of Supercharger Compressor for Cold Climate Air Source Heat Pumps

Thomas Walter
Mechanical Solutions, Inc., United States of America, tom.walter@mechsol.com

Travis Jonas
Mechanical Solutions, Inc., United States of America, travis.jonas@mechsol.com

Follow this and additional works at: https://docs.lib.purdue.edu/icec

DEVELOPMENT AND TESTING OF A NEW SUPERCHARGER COMPRESSOR FOR EXPANDED USE OF AIR-SOURCE HEAT PUMPS IN COLD CLIMATES

Thomas J. WALTER[1], Travis A. JONAS[2]

[1]Mechanical Solutions, Inc.
Albany, NY, USA
Telephone: (518) 320-8552, tjw@mechsol.com

[2]Mechanical Solutions, Inc.
Whippany, NJ, USA
Telephone: (973) 326-9920, travis.jonas@mechsol.com

ABSTRACT

The on-going development of a compact centrifugal compressor as a first stage or pre-compressor for cold climate operation of heat pumps is described. Positioned in the low pressure vapor portion of the refrigerant loop, this compressor will, on cold days, operate automatically to boost refrigerant pressure, in a manner similar to the way an automotive supercharger pressurizes air. The single stage motor driven centrifugal compressor runs on oil-free bearings. It is being configured to work in concert with a traditional heat pump compressor. The goal of this work is to enable air source heat pumps to efficiently extract heat from even the coldest ambient air without backup heat and without changing refrigerant type or the basic design of the positive displacement style compressors widely used in today's heat pumps. Doing so will allow air source heat pumps to operate effectively in virtually all major population centers. To date, a first article supercharger has been designed and built, and its performance mapped. Work to integrate it with a commercially available positive displacement (PD) heat pump compressor is underway.

1. INTRODUCTION

Electrically driven heat pumps are an effective method of extracting heat from ambient air. As air temperature falls, however, heat pump performance falls off, essentially limiting their year-round usefulness to warmer climates. In colder climates heat pump-equipped heating systems typically have a secondary means to provide heat, usually electric strip heaters. This adds complexity, duplication, cost and pollution. An air source heat pump system that maintains both capacity and coefficient of performance (COP) in cold climates could have a significant energy-savings impact, particularly where natural gas is not available.

For the US Department of Energy[1], Mechanical Solutions, Inc. (MSI) is developing key elements of an integrated refrigerant compressor system that efficiently extracts heat from very cold ambients. The goal is a system that requires zero backup heat in even the coldest climates, in effect achieving a viable heat pump furnace. The core innovation is a second compressor, in the low pressure portion of the refrigerant loop that will, on cold days, boost the refrigerant pressure. The goal is a compact, highly efficient pre-compressor that works in concert with a traditional heat pump compressor. Once developed, the market objective is heat pumps that can be applied to virtually all major markets without changing the type of refrigerant employed or the basic design of existing heat pump compressors. As sources of electric power become cleaner, expanded heat pump use offers the ability to produce heat with minimal increase in greenhouse gases. A heat pump that can efficiently function as a furnace, with no requirement for backup heat, will revolutionize major portions of the HVAC industry. A recent presentation at an International Energy Agency (IEA) Heat Pump conference (Walter 2014) describes the overall system and the thermodynamic role of the supercharger, which functions in a manner similar to automotive supercharger. The following sections describe technical aspects of the device, and test results to date.

---

2. APPLICATION

The DOE's performance targets for a cold climate air source heat pump includes a goal of efficient operation down to (-)25°C ((-)13°F). Although heat pump performance begins to wane as temperatures fall below the mid-forties, a number of models are capable of heat extraction to the mid-teens. The objective of the supercharger therefore is to begin operation in this temperature range, then run faster as ambient temperature falls, reaching max speed at the coldest ambient. To be of optimum value, the supercharger's outlet pressure should be fairly constant and matched to a (PD suction) pressure where the PD compressor has peak efficiency.

3. PROTOTYPE SUPERCHARGER

The pre-compressor consists of a single stage centrifugal compressor driven by a permanent magnet motor. Gas foil bearings (no moving parts, oil-free) support the rotating components. It is driven by a variable frequency drive (VFD). Figure 1 shows the principal parts.

Based on the duty cycle described above and with R410a (a commonly used HFC refrigerant in heat pumps) as the working fluid, these conditions were selected for compressor operation: Inlet Total Pressure = 234 kPaa (34 psia); Inlet Total Temperature = (-)27°C ((-)16°F); Total Pressure Ratio ≈ 3.3; Mass Flow Rate = 0.19 kg/s (24.8 lbm/min). Based on these correlations and loss models, a single stage compressor operating at a rotational speed of 100,000 rpm was selected. The compressor stage was modeled using a centrifugal impeller, vaned diffuser, and elliptical volute. This resulted in an impeller with 18 full height blades and zero partial height splitter blades, and a diffuser with 13 vanes. Based upon the analysis, the compressor was predicted to have a Total Adiabatic Efficiency = 0.72. Figure 2 shows the aero components.
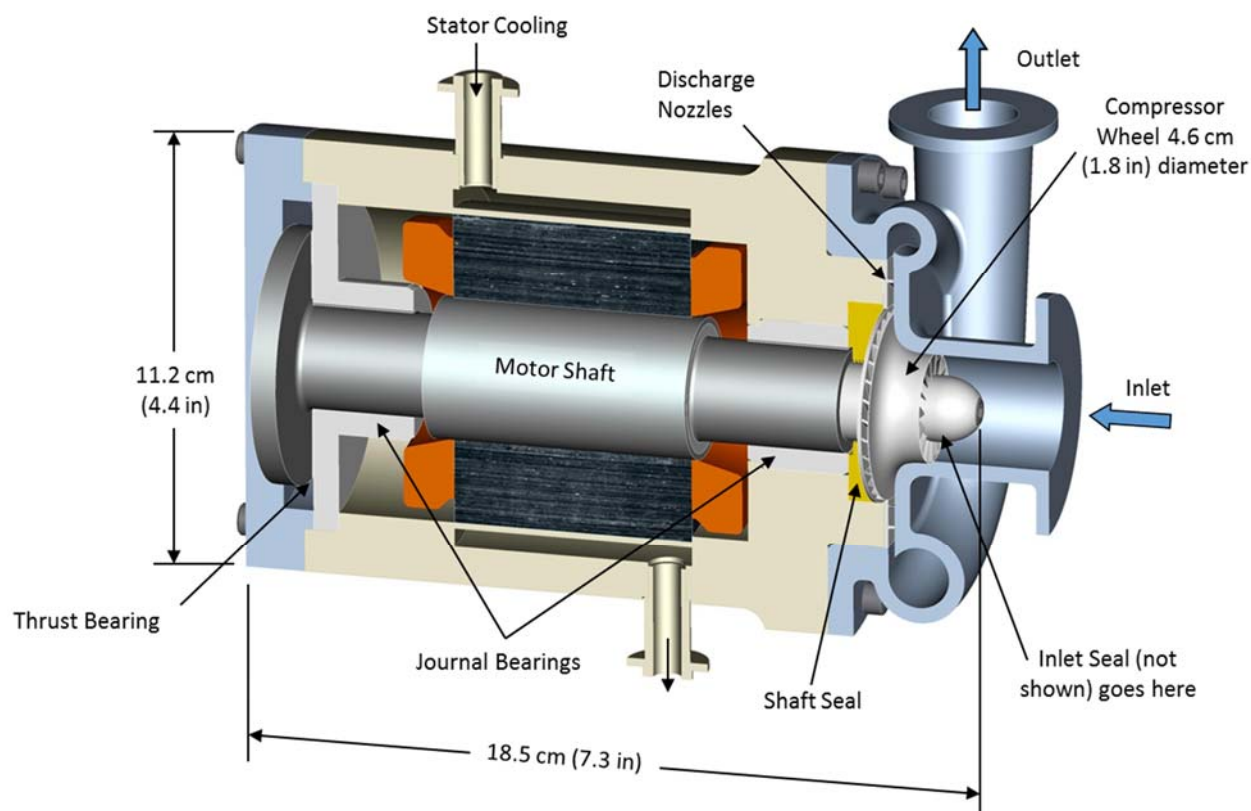
Figure 1: Supercharger for Pre-Compressing Refrigerant Vapors

Figure 2: Final Design and Prototype Aero Parts - Volute Housing (Top) Impeller (Middle) and Diffuser (Bottom)

The impeller, shaft, and attachment bolt were analyzed using finite element-based software to evaluate operating stress and modal characteristics, with satisfactory results.

4. MANUFACTURING METHODS FOR COMPRESSOR AERO COMPONENTS

Historically, manufacturing prototypes for these components is expensive and time-consuming, with components made using traditional machining, casting, or a combination of both processes. This involves initial development cost and lead time to produce the first article components, which were prohibitive for this project. To address this issue, MSI internally funded an effort to identify and evaluate alternative manufacturing techniques that are faster for prototypes and less expensive. *Additive manufacturing* and *rapid investment casting* were identified as two advancing technologies that offered much promise.

Additive Manufacturing: Also known as 3D printing, is growing in popularity and capability. Originally developed to create 3D shapes using thermoplastics and photopolymers, the technology is broadening and now includes a variety of metals. The process involves the use of a high energy beam, either laser or electron, which is focused on a bed of powder metal. Three processes currently used to fabricate metal components are Direct Metal Laser Sintering (DMLS), Selective Laser Melting (SLM), and Electron Beam Melting (EBM). Of the three processes, DMLS is the most commonly used and offers the best dimensional control and finish quality for small parts, and therefore was selected for manufacturing the impeller.

Rapid Investment Casting: Though the technology has been around for centuries, investment casting has recently been able to make improvements in reducing initial cost and lead times by taking advantage of additive manufacturing technology. The process involves building the pattern for the molds directly from a CAD file using a 3D printing process, such as Stereolithography (SLA) or Selective Laser Sintering (SLS). Lead times are reduced to days versus 8 to 10 weeks for standard investment castings. Parts are limited in size to those that can be built with the additive manufacturing process, but in some cases sections can be built and joined together to produce larger parts. Because of its size, the volute housing was manufactured using the rapid investment casting process.

Material Assessment: Although the DMLS process possesses many advantages, concerns exist regarding the strength and surface quality of the sintered power metal. For the impeller, a precipitation hardened stainless steel, 17-4PH heat treated to the H900 condition was selected for its high tensile strength. To evaluate the tensile properties of the sintered material, three tensile test specimens were fabricated and processed identically along with the impellers. These specimens were then tested to failure and the results compared to the specifications for wrought and cast material, as listed in Table 1. The results show the sintered material exceeded the minimum strength requirements for both wrought and cast material. The sintered material exhibits slightly lower ductility than wrought material, but better ductility than cast material. In addition, one of the finished impellers was successfully spin-tested to 115,000 rpm (15% over-speed) without failure.

Impeller Surface Finish: Ideally, surfaces exposed to high velocity gas flows should be as smooth as possible to minimize turbulence and friction losses. A surface finish of 0.81μm (32 μin) or better is preferred. As processed, the DMLS material exhibits a surface finish of 3.3 μm (130 μin). Accessible surfaces can be improved through bead blasting or polishing, however, the presence of the shroud prevents direct access to the blades. Alternate polishing methods were explored to improve the surface finish of these inaccessible areas, including electro-polishing, electro-plating, and extrusion honing. Of these, electro-polishing was determined to be the most likely to improve the surface finish most uniformly with minimal impact on dimensional tolerance. One of the impellers was sent to an electro-polishing vendor, who adjusted process parameters to optimize the process but with marginal results.

Table 1: Tensile Test Results Comparing DMLS Produced Samples to Other Forms

DMLS Data

Specimen ID	Ultimate Tensile Strength		0.2% Offset Yield Strength		% Elongation	% Reduction in Area
	MPa	ksi	MPa	ksi		
SN1	1434	208	1282	186	5	11
SN2	1448	210	1358	197	7	8.5
SN3	1455	211	1331	193	9	15

Published Data (minimum values)

|						
Wrought	1310	190	1172	170	10	35
Investment Cast	1241	180	1103	160	4	12

While improvement was realized in some sectors, other areas were worsened, with the process creating localized pitting. The vendor attributed the varying result to the non-uniform nature of the sintered material. It was therefore decided to proceed with the as-manufactured surface finish and accept the aero performance degradation for initial testing. Methods of producing the impeller in two pieces (i.e., a separate shroud), enabling full access to the blade surfaces prior to attaching the shroud, can be explored later. As related below, initial testing revealed an adiabatic efficiency of 0.68 vs. the above-noted prediction of 0.72. We view this result as quite acceptable for a first prototype, with impeller surface finish and the type of seals implemented (see discussion below) deemed the principal contributors to the difference observed.

Volute Housing Fabrication: Initially we planned to make the volute housing from 17-4PH stainless steel, the same material as the impeller. However, the casting vendor ran into difficulties getting uniform flow through the thin-walled sections of the casting. Since the strength of 17-4PH is not required for the volute housing, the material was changed to A-356 aluminum, an alloy with superior casting properties. The result was a complete success, with the end product shown in Figure 2. To verify the aluminum casting had adequate strength, the housings were successfully hydro-tested to 1.03 Mpa (150 psi) (150% of the working pressure).

Diffuser Fabrication: We used traditional machining methods for this part, using Grade 304 stainless steel.

5. MOTOR AND CONTROLLER

Two motor types (Induction and Permanent Magnet) were evaluated. A permanent magnet (PM) style was selected for the prototype since it results in a smaller, higher efficiency motor. Based on an assessment of parasitic losses, a 100,000 rpm 4-pole motor with nominal rating of 10 kW (13 hp) was selected. It contains stator laminations that are 0.178 mm (0.007 in) thick and copper windings, with a predicted efficiency of 96.9 percent. Figure 3 shows a completed stator and shaft. A commercially available digital drive variable frequency drive (VFD) which operates without the need for a Hall Effect sensor was selected.
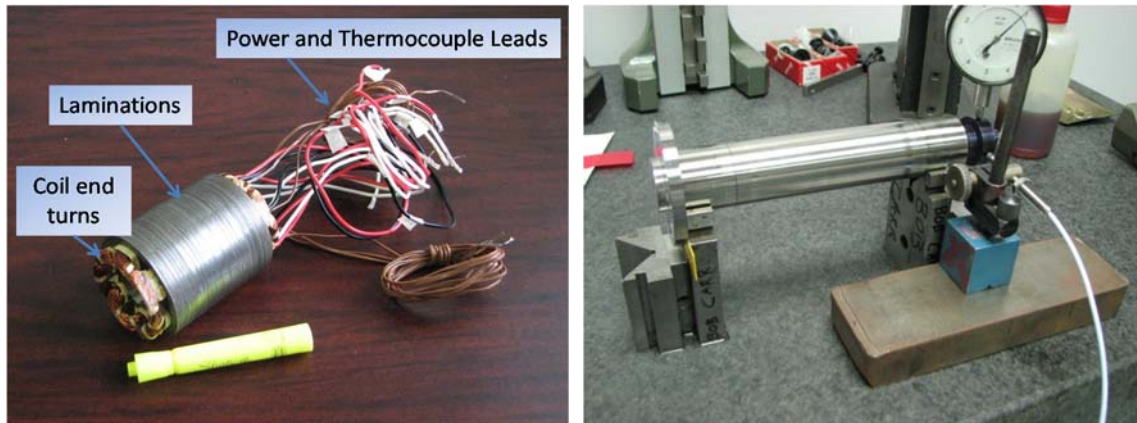
Figure 3: Motor Stator and Shaft

6. BEARINGS AND SEALS

A parametric design study was conducted to size the gas foil bearings. Load capacity was determined over a range of bearing lengths and diameters at 100,000 rpm. Once the final designs related above were complete, the bearing sizes were finalized as follows: Both radial bearings are 3.3 cm (1.3 in.) diameter x 2.5 cm (1 in.) long. This results in a more-than-adequate 58 N (13 lbf) load capacity per bearing for the vertically mounted machine. The single acting thrust bearing has a 6.4 cm (2.5 in.) OD and 3.8 cm (1.5 in.) ID with 6 pads of approximately 60° arc angle per pad. The load capacity of this bearing is 245 N (55 lbf), which is ample to carry the weight of the rotor and anticipated compressor thrust load.

In small centrifugal compressors, sealing around the impeller is an especially key part of overall machine performance. As shown in Figure 1, there are two principal dynamic seals in the supercharger: At the impeller inlet, and on the shaft behind the impeller. For initial operation, labyrinth seals have been implemented at both locations. Labyrinth seals are commonly used in turbomachinery. They provide a close-clearance but non-contacting seal, so there is a small amount of flow (leakage) through the seal. In a large compressor such leakage is generally of no consequence. In small machines however, this leakage can be a significant portion of the total flow. At the shaft seal, a small amount of purposeful flow through the seal cools the motor and bearings by passing refrigerant through the bearings and motor-stator gap. As operational experience is gained, we will consider alternate inlet seal configurations that may moderately improve supercharger efficiency. A potential downside associated with some higher-performance seals is their potential to introduce small forces on the shaft that could degrade the dynamic stability of the supercharger's suspension system. It should be noted that all flow through the seals is retained within the sealed refrigerant system and merely recompressed; there is no "leakage" in the traditional sense. Figure 4 shows a set of bearings and seals.

Figure 4: One Set of Bearings with Thermocouples Attached (left) and Seals (right)

Rotordynamics: Compared to most other bearing types, gas foil bearings have lower stiffness and lower load carrying capability. As part of the design process, initial predictions were made to confirm no critical speeds within the anticipated operating speed range. With all key aspects of the rotor and bearings established, a final rotordynamic evaluation of the rotor was performed to predict critical speeds and their mode shapes. The main portion of the shaft is a high-strength alloy steel. The magnets are neodymium-iron-boron, segmented into three pieces axially and four pieces circumferentially. The magnets are bonded to the shaft with epoxy and held in compression with an Inconel sleeve which is installed with a heavy interference fit.

The analysis was performed using the journal bearing stiffness values generated by one of MSI's proprietary foil bearing codes. These values, the rotor geometry, and impeller mass properties, were input into modeling software to determine rotor critical speeds and mode shapes. To be conservative, the motor magnet assembly was not included in the stiffness calculation, although its mass was included. Including a stiffness allocation would tend to raise the first bending critical speed (third overall critical speed).

The results of the rotordynamic analysis for the first three modes are summarized in Table 2 for running speeds of 50,000 and 100,000 rpm[2]. A conservative approach is to achieve a design wherein the rigid body modes are below the machine's minimum operating speed, and the bending modes are comfortably above the maximum operating speed. In this case, the rigid body modes were predicted to occur well below the supercharger's minimum operating speed of 85,000 rpm. The predicted first bending critical was well above the machine's 100,000 rpm max speed.

As discussed below, Table 2 also shows the approximate critical speeds actually observed in the test data. For modes 1 and 2, the predicted vs. actual differences are attributed to lower bearing stiffnesses due to smaller shaft displacements and bearing loads than those used in the analysis. For mode 3, the difference is likely due to higher overall shaft stiffness, owing to a contribution from the magnet attachment method.

Table 2: Predicted and Actual Critical Speeds (in rpm) of the Rotor

| Mode Number	Mode Shape	@ 50 krpm	@ 100 krpm	Observed During Test
1	Rigid Body	23,430	24,450	15,000
2	Rigid Body	28,800	31,400	18,000
3	Bending	143,720	146,970	154,000

7. INITIAL TESTING AND RESULTS

An in-house vapor-only test loop to assess compressor performance was designed and built. In addition to flow meters, accumulators and instrumentation to measure performance and vibration, this loop includes heat exchangers to remove the compression heat added by the supercharger. A data acquisition system gathers 30+ channels of process and dynamic data in real time.

Initial tests involved grooming the motor controller. This was followed by scoping runs with a vane-less impeller, dummy housing, and air not refrigerant in the loop, to confirm rotordynamic performance. For these tests, additional instrumentation was in place, including eddy current displacement sensors to observe shaft motion at all speeds.

Shaft displacements were quite low at all speeds, nominally 5.1μm (0.0002) inches zero-peak when compensated for runout.[3] Figure 5 shows shaft orbits at the lower (Compressor end) and upper (Thrust Bearing end) regions of the Supercharger at various speeds. The four-lobe pattern in the uncompensated orbits is attributed to A) the effect (magnetic influence or actual shaft motion) of the 4-pole motor, or (more likely) B) the effect of the shims (4 in

---

[2] The shift up in speed is the result of several effects, including increase in bearing stiffness as a function of speed, and gyroscopic stiffening.

[3] The term runout refers to local-to-the-sensor surface and near-surface discontinuities, and small variations in the shaft's mechanical and electrical properties, which are detected by this type sensor, in addition to the dynamic movement of the shaft. "Compensated" means these effects have been vectorally subtracted from the overall data, leaving only the dynamic data, which is of primary interest here.
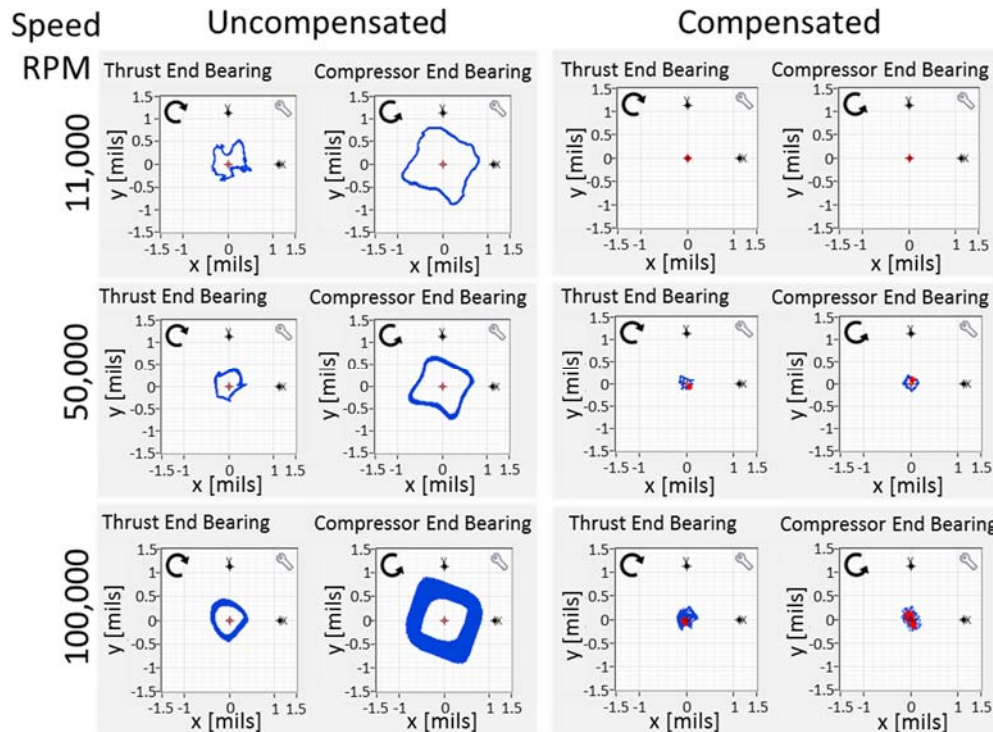
Figure 5: Shaft Orbits at Three Speeds, with (right side) and without (left) Compensation for Runout

number, 90 degrees apart) installed in the radial bearings, a common method used to preload gas foil bearings in vertically mounted machines. The "fat" orbits at the highest running speeds are attributed to data sampling rate limitations. An oscilloscope directly observing sensor outputs confirmed narrower orbits at all speeds.

Confirmation of Rotordynamics: The rigid body critical speeds occurred in the 15,000 rpm range, lower than predicted. As noted above, the discrepancy is attributed to the low shaft displacements, which results in lower bearing stiffnesses and therefore lower critical speeds. Figure 6 shows shaft displacements (uncompensated for runout) through the 15,000 rpm (250 Hz) range were comfortably low, indicating a good amount of damping in the bearings.
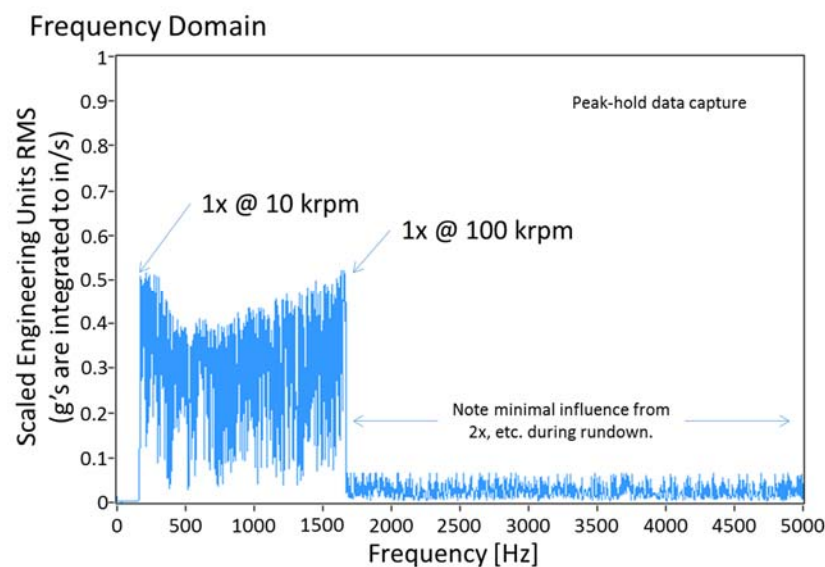
Figure 6: Compressor End Vibration, mils$_{rms}$, During Rundown from 100,000 rpm to 10,000 rpm; No Runout Compensation

Subsynchronous Vibration: At speeds above 90,000 rpm, a low level subsynchronous was observed, at a frequency equivalent to the rigid body criticals, see Figure 7. Once encountered, the subsynchronous did not increase significantly in amplitude as running speed was increased to max. Once present, the subsynchronous was discernable, at low amplitudes, until the running speed was dropped below 50,000 rpm. This phenomenon, sometimes labeled a controlled instability, is not unusual for shafts running on gas foil bearings.
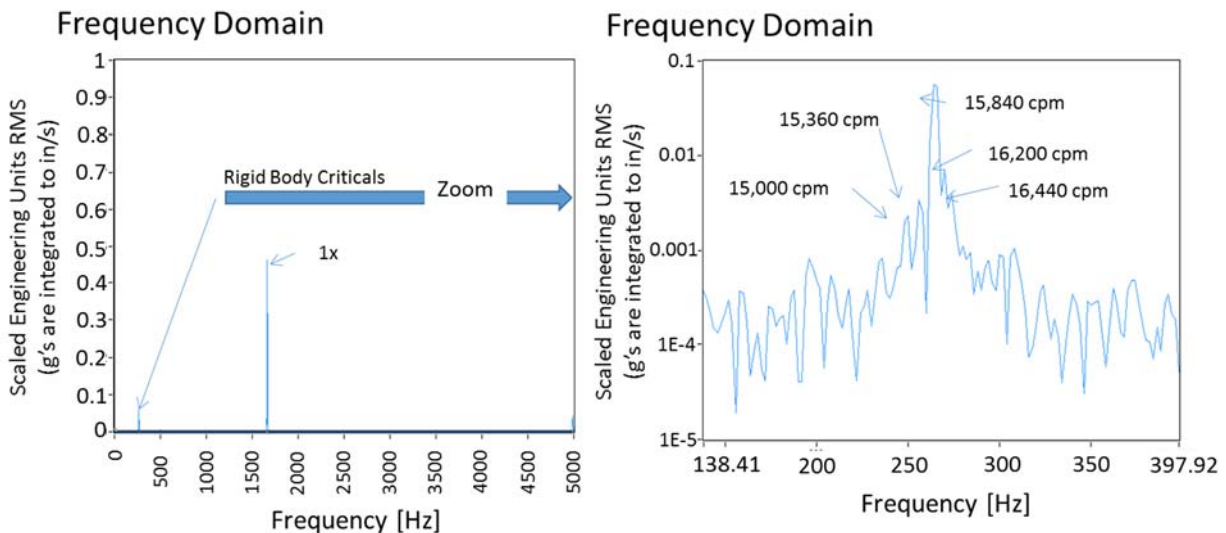
Figure 7: Compressor End Shaft Displacement, mils$_{rms}$ @ 100,000 rpm; No Runout Compensation

Damping Determination: An important aspect of the dynamics of high speed machinery is the amount of damping present at the bearings, as low damping can cause dynamic stability issues. Instability often results in excessive vibration and sometimes machine failure in short order. Gas foil bearings generally have lower damping than most other types of hydrodynamic bearings. Combining this aspect with the usual situation where a foil bearing-supported machine operates at speeds many times higher than the machine's rigid body critical speeds makes damping the most critical ingredient for successful machine operation.

For these reasons, we elected to experimentally determine the amount of damping in the supercharger's rotor-bearing system by implementing a commonly used "ring-down" method. Specifically, with the supercharger running, the motor housing was tapped with a hammer while observing lateral displacement of the spinning shaft at the shaft displacement sensors. Figure 8 shows a typical response, with these average results: Log Decrement = 0.64; damping ratio = 0.1; amplification factor = 5.
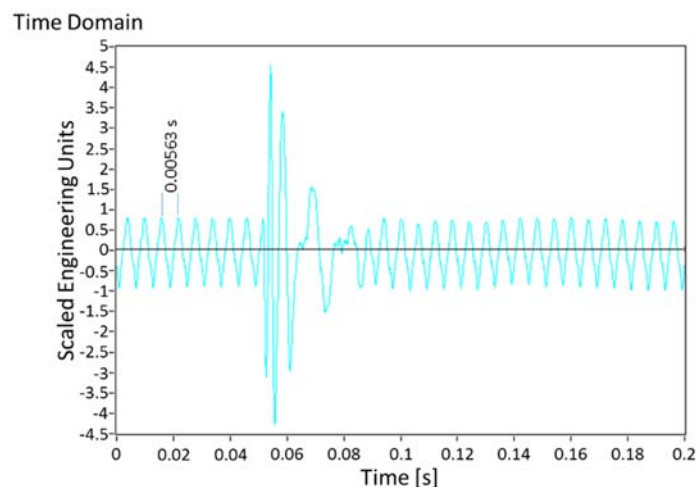

Figure 8: Compressor End Shaft Displacement, mils$_{rms}$ @ 10,000 rpm; No Runout Compensation

With these tests complete, the vane-less impeller was switched out for the bladed impeller, diffuser and shaft seal but not the volute or inlet seal. This configuration was run to max speed to verify no significant changes in vibration or rotordynamics, and none were observed. The test loop was then re-plumbed for refrigerant, and the supercharger's test housing switched out for the volute and inlet seal. During the impeller change-out, the motor internals and bearings were inspected and found to be in excellent condition, with only minor wear-in marks noted. The supercharger was reassembled using the same bearings.

Aero Performance: Test runs to map as-built performance were conducted in late 2013 and early 2014. Figures 9 and 10 relate performance data from all of the runs conducted to date. Figure 9 shows the results as generally depicted for centrifugal compressors. For this style compressor, optimum operation is obtained when running through the center of the "islands" of constant efficiency. Figure 10 shows the corresponding head vs. flow coefficients, which can be used to assess how the compressor will perform in other applications. Both figures show encouraging data, with consistent results, reasonably shaped performance curves, and excellent data point clustering. Although somewhat lower than predicted, both head and flow coefficients are quite acceptable for a first prototype. As noted above, this initial build included purposeful simplifications regarding seal type and impeller finish. The Operating Line shown in Figure 9 represents current plans for supercharger operation when combined with a commercially available PD compressor. The region above the top end of the Operating Line is being reserved as margin to fine tune compressor interoperation, if needed.
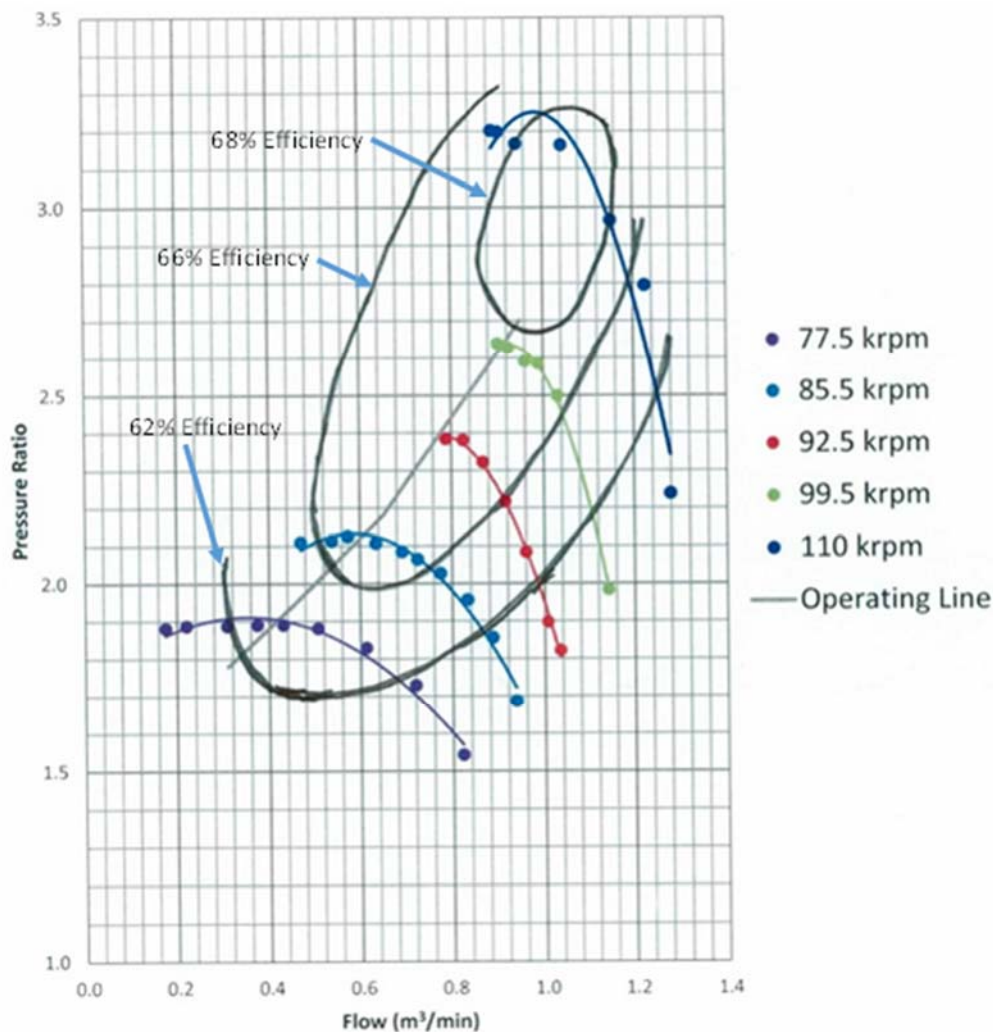
Figure 9: Compressor Performance Map for First Article, and anticipated Operating Line
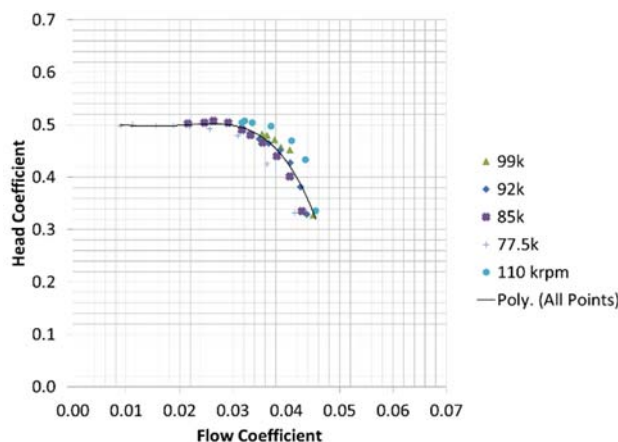
Figure 10: Head and Flow Coefficients for First Article Compressor

Other Performance Metrics: Motor housing vibration levels were typically 0.51 mm/sec$_{rms}$ (0.02 in/sec$_{rms}$) or less. Acoustic (airborne) sound levels were not measured but observed as principally a low-level tone, likely associated with impeller vane or blade pass, at speeds above 50,000 rpm. Thermally, bearing losses were in line with predictions. Windage and stator losses were somewhat higher than expected.

8. PRESENT STATUS AND PLANS

As presently configured, the prototype supercharger is suited for a heat pump in the 45 kW (150,000 Btu/hr) class, with a reasonable COP$_h$ of 2.32. Work is underway to complete the DOE SBIR grant work scope by marrying the supercharger to a properly sized PD compressor and demonstrating effective solo and simultaneous operation of both compressors on our in-house test loop. Within the constraints of remaining schedule and budget, we are also implementing hardware modifications to reduce windage and motor losses.

Follow on work includes an anticipated grant from the State of New York to configure the compressors with associated heat exchangers, fans, and associated controls to fashion the components of a cold climate heat pump for demonstration to interested third parties, including heat pump OEMs, who have direct access to end users and are well suited to establish the bottom line economics needed for a viable cold climate heat pump[4]. This work is expected to commence in spring 2014.

Other potential uses for the refrigerant pre-compression concept described herein include industrial and commercial coolers, chillers and freezers as a compact and energy-efficient alternative to existing methods, with the potential for increased capacity or lower temperature operation.

9. CONCLUSION

Centrifugal compressors are used throughout industry because they have fewer rubbing parts, are relatively energy efficient, and give higher flow than a similarly sized reciprocating compressor or positive-displacement compressor. However, they cannot achieve the high compression ratio of reciprocating compressors without multiple stages. In many respects, the application discussed herein makes optimum combined use of both compressor types. It is concluded that work conducted to date has verified the underlying design of a motor driven supercharger to improve the cold-day performance of air source heat pumps.

References:

Walter, Thomas J., 2014, Supercharger for Heat Pumps in Cold Climates, *11th Biennial IEA Heat Pump Conference.*

---

[4] New York Energy Research and Development Authority Grant number 34903 "Supercharger for Cold Climate Heat Pumps".